Self-consistency in force-free modelling, and chromospheric constraints

Michael S. Wheatland
University of Sydney

ISSI International Team Workshop
3-7 October 2022

THE UNIVERSITY OF SYDNEY

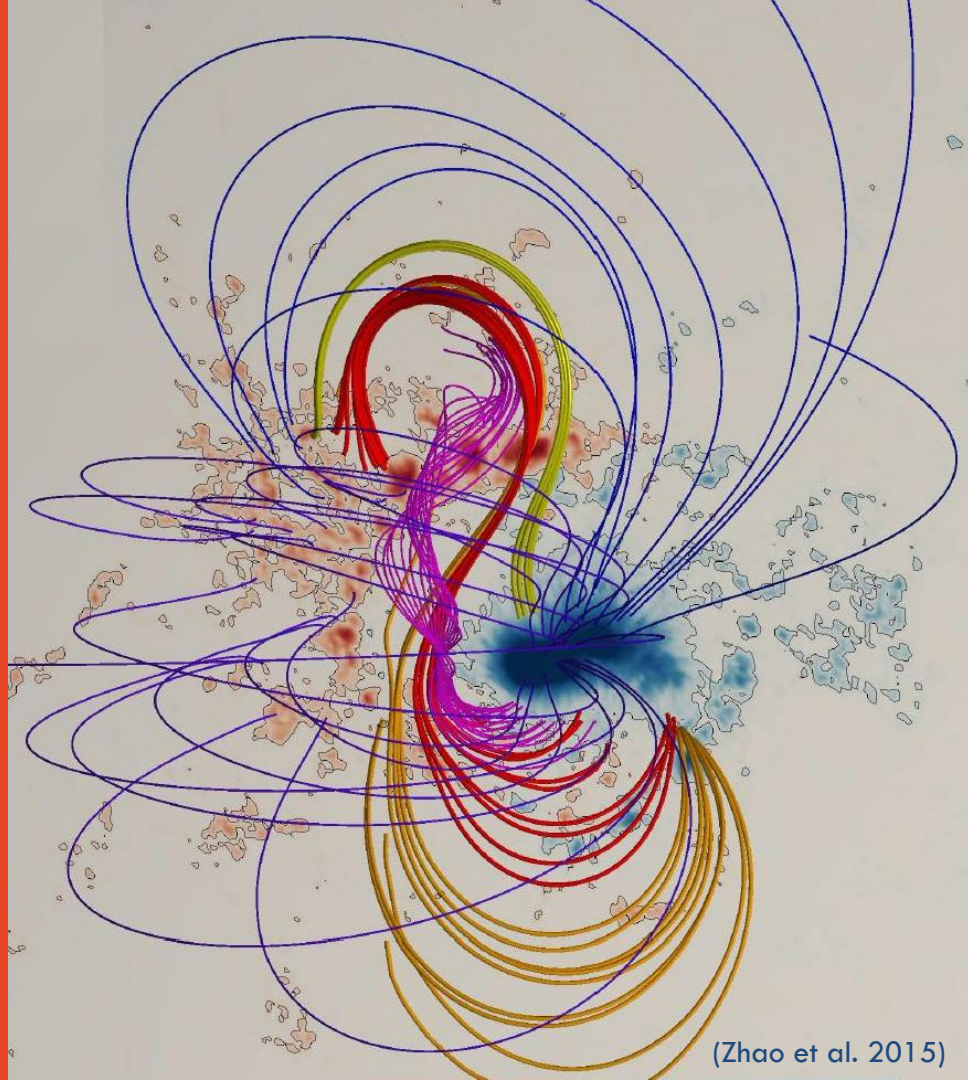

(Zhao et al. 2015)

A hierarchy of models

Static/data-constrained

Time-dependent/data-driven

Nonlinear force-free (NLFF)

a boundary value problem for $\boldsymbol{B}$

Magneto-hydrostatic

a boundary value problem for $\boldsymbol{B}$, p, ρ

Magneto-frictional (MF)

a boundary value problem for $\boldsymbol{B}$ or an initial value/

boundary value problem for $\boldsymbol{B}$

Zero-β magneto-hydrodynamic (MHD)

an initial value/boundary value problem for $\boldsymbol{B}$, $\boldsymbol{v}$ and ρ

Full MHD

an initial value/

boundary value problem for $\boldsymbol{B}$, $\boldsymbol{v}$, p and ρ

Increasing physics and computational cost →

NLFF extrapolation enables many studies

- Examples of the use of NLFF reconstruction

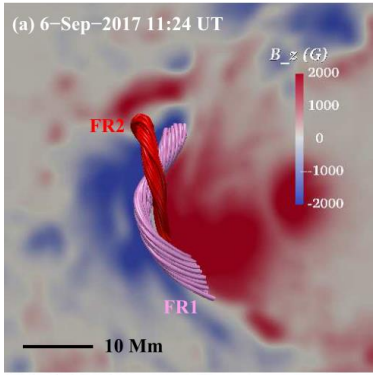

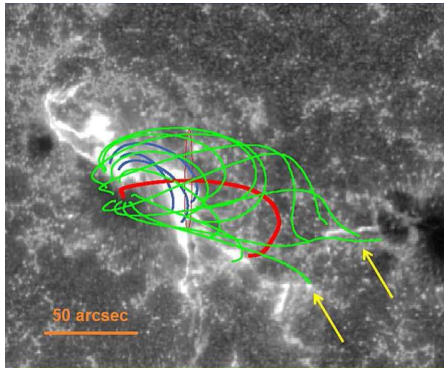

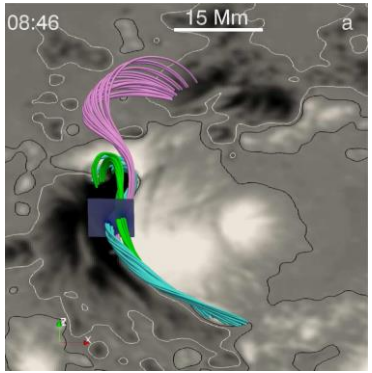

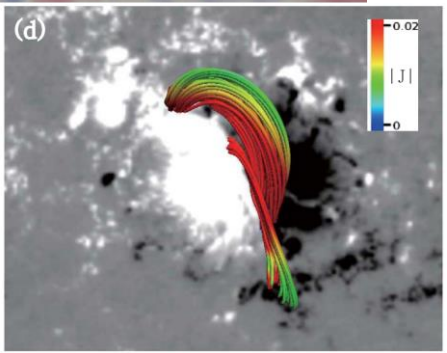

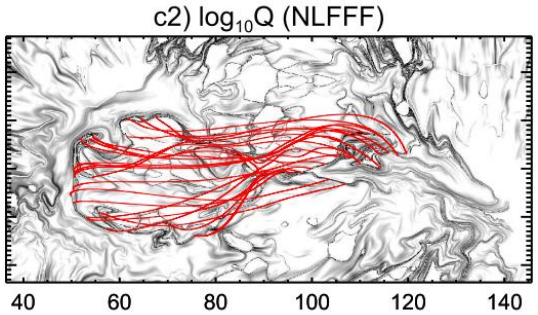

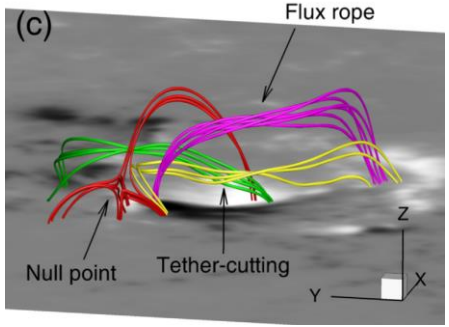

Clockwise from top left:
Hou et al. (2018);
Kuroda et al. (2018);
Liu et al. (2018);
Zou et al. (2019);
Su et al. (2018);
Kang et al. (2019)

The NLFF model

- The nonlinear force-free model for a magnetic field $\boldsymbol{B}$ is:
  (Wiegelmann & Sakurai, Living Reviews of Solar Physics 2012)

$$\boldsymbol{J} \times \boldsymbol{B} = 0 \quad \text{and} \quad \operatorname{div} \boldsymbol{B} = 0 \tag{1}$$

  - where $\boldsymbol{J} = \mu_0^{-1} \nabla \times \boldsymbol{B}$ the electric current density
- Writing $\boldsymbol{J} = \alpha \boldsymbol{B}/\mu_0$ ($\boldsymbol{J}$ is parallel to $\boldsymbol{B}$):

$$\boldsymbol{B} \cdot \nabla \alpha = 0 \quad \text{and} \quad \nabla \times \boldsymbol{B} = \alpha \boldsymbol{B} \tag{2}$$

  - where α is the force-free parameter
- Methods of solution of Eqs. (2) are iterative
  - Grad-Rubin iteration (Grad & Rubin 1958; Amari et al. 2006; Wheatland 2007)
  - optimization (Wheatland, Sturrock & Roumeliotis 2000; Wiegelmann 2008)
  - magneto-frictional method (Chodura & Schlueter 1981; Valori et al. 2005)

The BCs on the NLFF model

- The boundary conditions for Eqs. (2) in $z \geq 0$ are:
  - B_z at $z = 0$
  - α at $z = 0$ over one polarity of B_z (labelled P, N)
- Some solution methods use the full vector $\boldsymbol{B}$ in the boundary
  - which is an over-prescription
- Vector magnetograms provide values of B_z and

$$\alpha = \frac{1}{B_z}\left(\frac{\partial B_y}{\partial x} - \frac{\partial B_x}{\partial y}\right) \tag{3}$$

  - values of α are available over both polarities of B_z
  - so the problem is over-prescribed
- Magnetogram data are inconsistent with the force-free model
  - necessary conditions for a force-free field are not met (Molodenskii 1969)

The Grad-Rubin method

Grad and Rubin 1958; Amari et al. 2006; Wheatland 2007

- Nonlinear PDEs solved via iterative solution of linear PDEs
  - a fixed point of the iteration is a solution to the force-free equations
- This method has the advantage of implementing the correct BCs for the model
- This method has also been generalised to magneto-hydrostatic modelling Gilchrist et al. 2016
  - that is the context of the G&R paper

Iteration scheme:

$$\begin{aligned} \nabla \times \mathbf{B}^{k+1} &= \alpha^k \mathbf{B}^k \\ \mathbf{B}^{k+1} \cdot \nabla \alpha^{k+1} &= 0 \end{aligned}$$

Boundary conditions:

$$B_n = \hat{\mathbf{n}} \cdot \mathbf{B}$$

$$\alpha \text{ where } B_n > 0 \ (P)$$

$$\textit{or} \text{ where } B_n < 0 \ (N)$$

Effects of inconsistency in NLFF modeling

- Origins of the inconsistency of the data and the model:
  - errors in measurements and field inference (e.g. Leka et al. 2009)
  - non-magnetic forces at the dense photosphere (Metcalf et al. 1995; Liu et al. 2013)
- Effects of inconsistency on NLFFF solutions
  (Schrijver et al. 2006; Metcalf et al 2008; Schrijver et al. 2008; DeRosa et al. 2009, DeRosa et al. 2015)
  - results produced by NLFFF codes may:
    - P1: not be accurate solutions to the NLFFF model
    - P2: disagree with other methods of solution, for the same BCs
    - P3: disagree with equally valid results for the same method
- P1: inaccurate results
  - the optimization method may produce results with $\mathrm{div}\,\boldsymbol{B} \neq 0$
  - "preprocessing" does not fix this (DeRosa et al. 2015)

Effects of inconsistency in NLFF modeling

- P1: Non-zero divergence can lead to inaccurate free-energy values

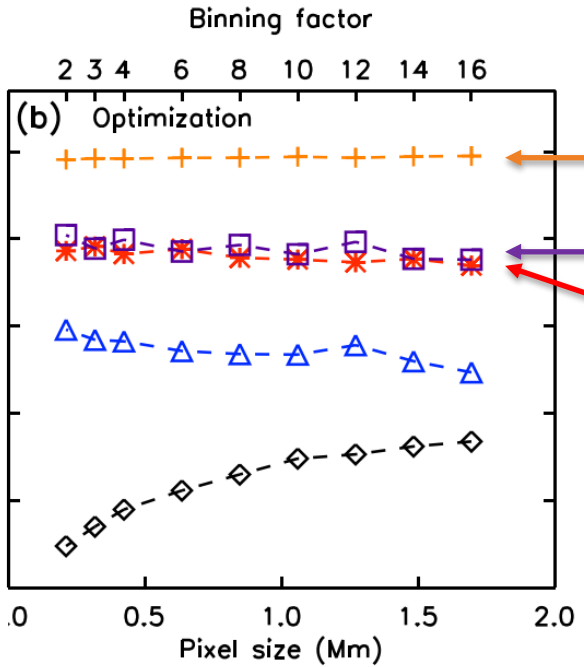

Potential field energy

Non-physical energy due to non-zero divergence

Free energy

$\tilde{E}_{0,s}$ $\tilde{E}_{J,s}$ $\tilde{E}_{0,ns}$ $\tilde{E}_{J,ns}$ $|\tilde{E}_{mix}|$

(DeRosa et al. 2015 using Valori et al. 2013 procedure)

Effects of inconsistency in NLFF modeling

- P2: different results from different methods
  - Grad-Rubin, optimization, magneto-frictional results may differ
  - they may have different energies, and field line structures

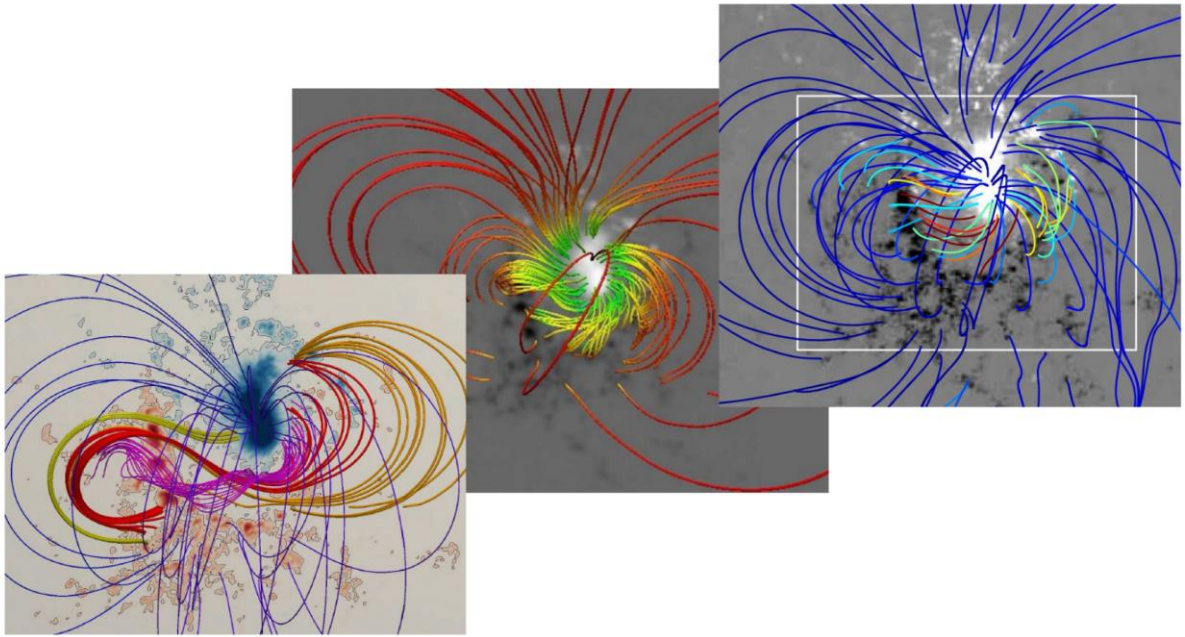

Three NLFFF models for AR12158 on 10 September 2014 (Zhao et al. 2016; Vemareddy et al. 2016; Duan et al. 2017).

Effects of inconsistency in NLFF modeling

- P3: two different results from the same method
  - Grad-Rubin codes solve a well-posed boundary value problem
    - which avoids unphysical solutions
    - but the vector magnetogram data provide two sets of boundary conditions

AR 12017 on 29 March 2014 (Mastrano, Yang & Wheatland 2020)

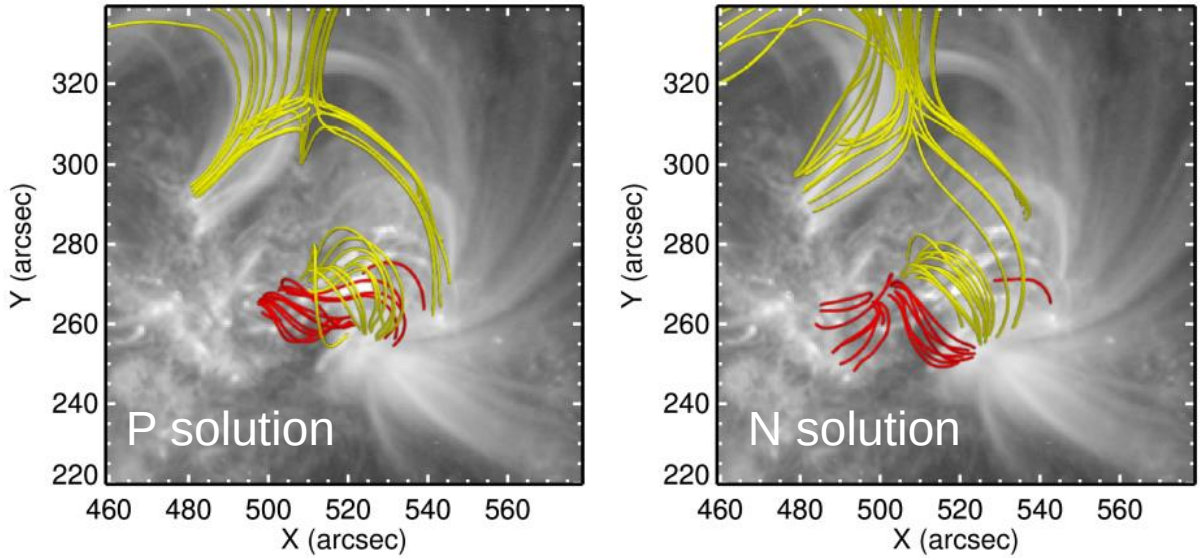

Self-consistency procedure

- The P and N solutions contain two distinct sets of boundary α values
  - which may be combined iteratively to arrive at consistent BCs
    - following the "self-consistency procedure"
      (Wheatland & Régnier 2009; Wheatland & Leka 2011)

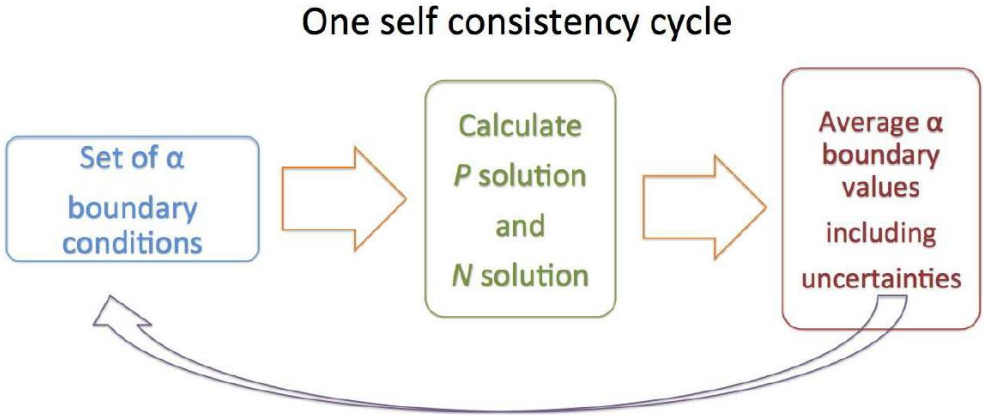

- The self-consistent solution has (cf. vector magnetogram):
  - the same BCs on B_z but modified (self-consistent) BCs on α

An improved self-consistent solution (Mastrano, Yang & Wheatland 2020)

- If the BCs are highly inconsistent, the self-consistent solution is close to potential

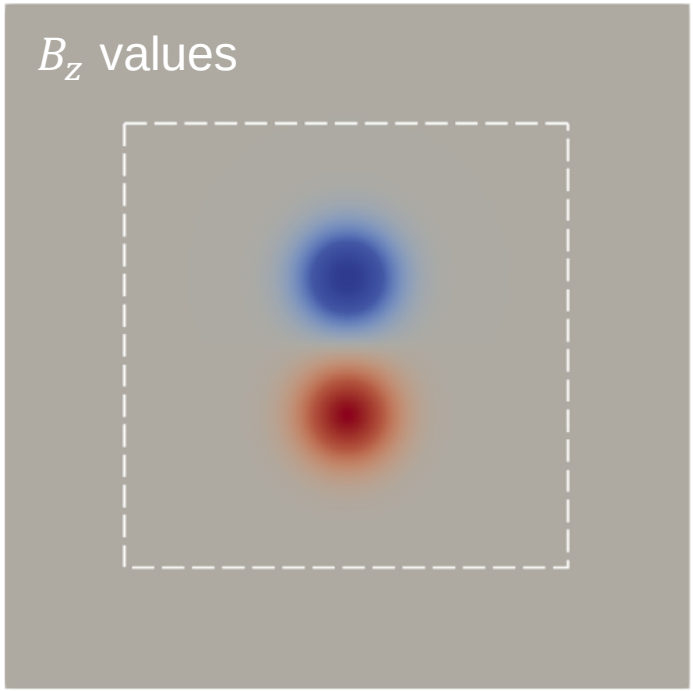

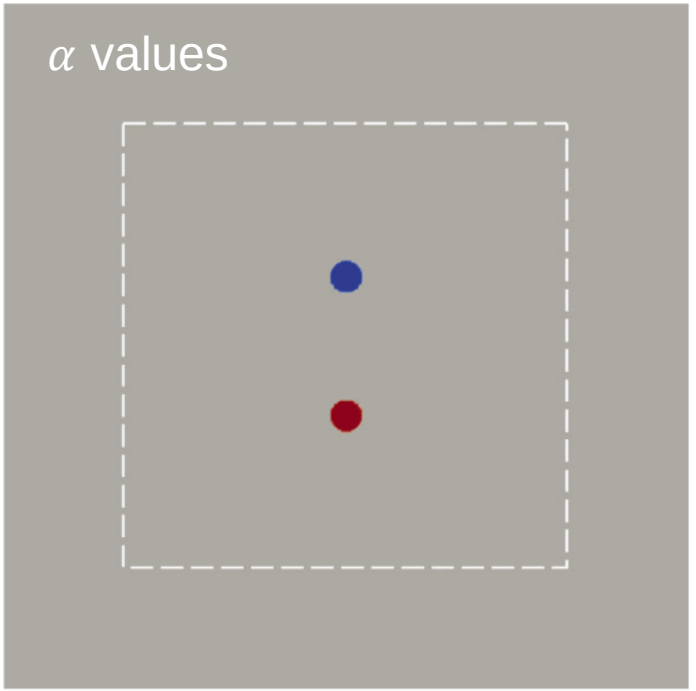

An improved self-consistent solution (Mastrano, Yang & Wheatland 2020)

- If the BCs are highly inconsistent, the self-consistent solution is close to potential

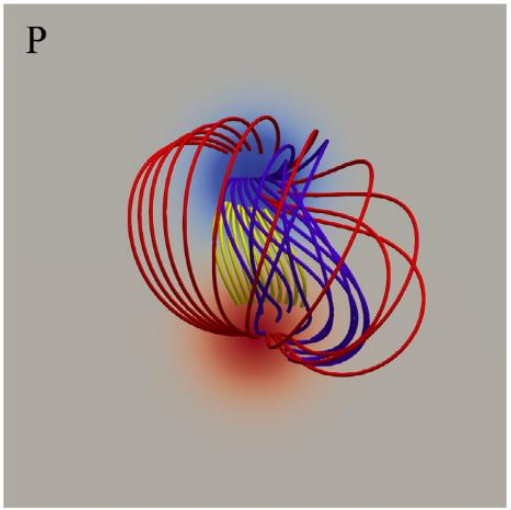

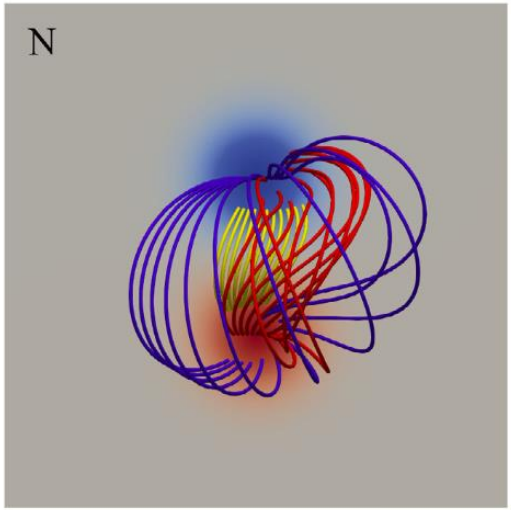

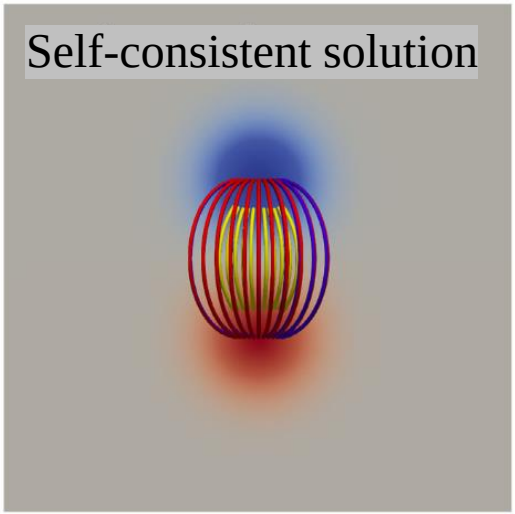

An improved self-consistent solution (Mastrano, Yang & Wheatland 2020)

- We can choose between the BCs on the polarities with weighted uncertainties σ

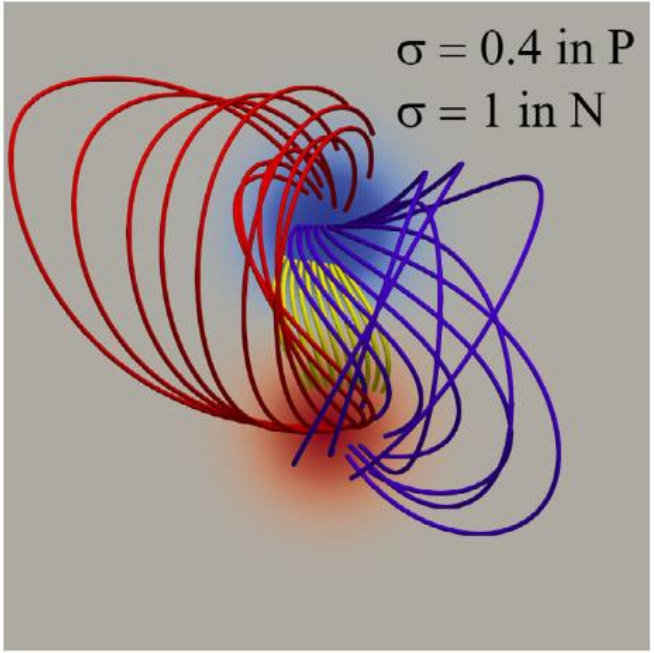

An improved self-consistent solution

- Weighting the α boundary values can e.g. preserve a flux rope

(Mastrano, Yang & Wheatland 2020)

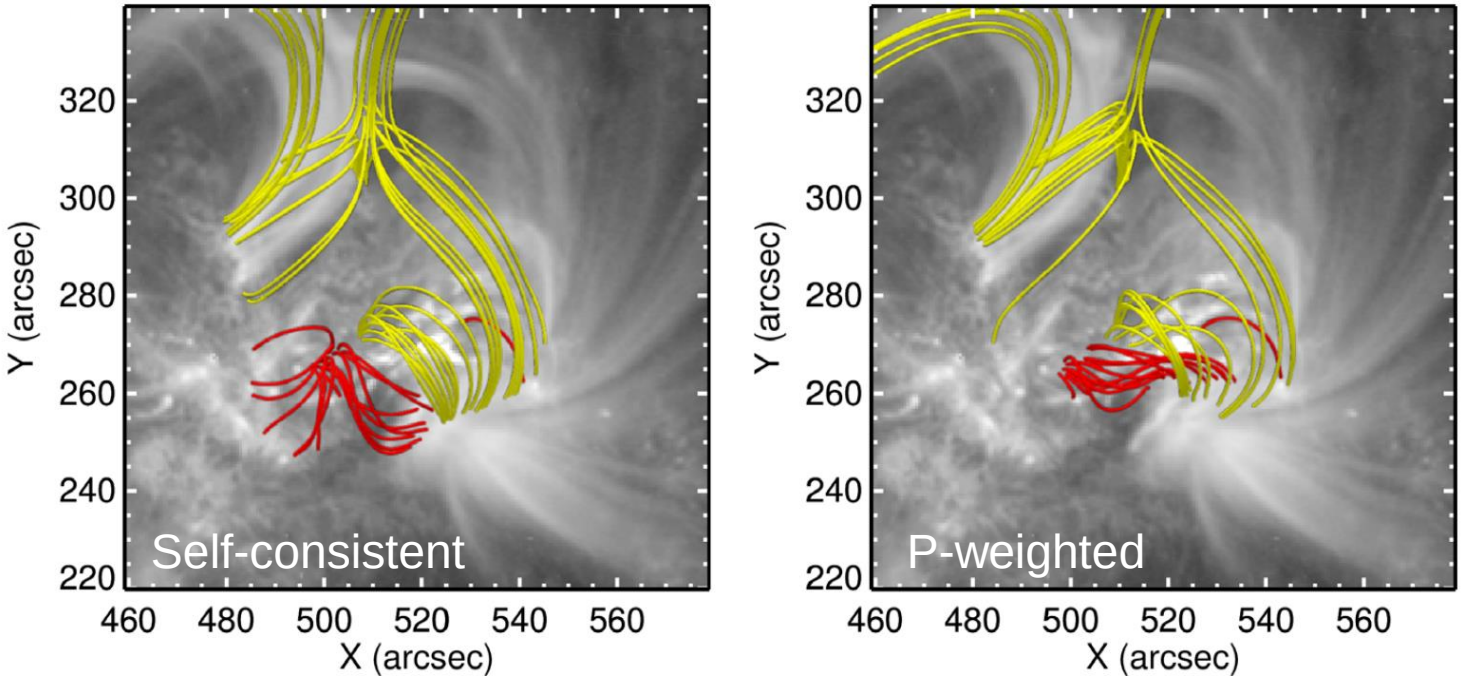

The divergence problem

- A departure from div $\boldsymbol{B} = 0$ can affect the energy of the field
  - the contribution of non-solenoidality to energy can be calculated (Valori et al. 2013)
- There is a very simple check on the reliability of a free-energy estimate
  - decompose the field into a potential and a non-potential component:

$$\boldsymbol{B} = \boldsymbol{B}_\mathrm{p} + \boldsymbol{B}_\mathrm{j} \quad \text{with} \quad (\boldsymbol{B} - \boldsymbol{B}_\mathrm{p}) \cdot \widehat{\mathbf{n}} = 0 \quad \text{on} \quad \partial\mathcal{V}$$

  - then calculate:

$$W_1 = \frac{1}{2\mu_0} \int \boldsymbol{B}_\mathrm{j}^2 \, \mathrm{d}\mathcal{V} = \frac{1}{2\mu_0} \int (\boldsymbol{B} - \boldsymbol{B}_\mathrm{p})^2 \, \mathrm{d}\mathcal{V}$$

$$W_2 = \frac{1}{2\mu_0} \int \boldsymbol{B}^2 \, \mathrm{d}\mathcal{V} - \frac{1}{2\mu_0} \int \boldsymbol{B}_\mathrm{p}^2 \, \mathrm{d}\mathcal{V}$$

  - the relationship is $W_1 - W_2 = \dfrac{1}{\mu_0} \int \phi \nabla \cdot \boldsymbol{B} \, \mathrm{d}\mathcal{V}$
  - hence a difference implies a non-solenoidal component

(Su et al. 2014; Moraitis et al. 2016; Mastrano et al. 2018)

The divergence problem (Gilchrist et al. 2020)

- A common metric for average div $\boldsymbol{B}$ of a data cube is:

$$\langle |f_i| \rangle = \left\langle \frac{\left| \int_{\partial S_i} \boldsymbol{B} \cdot d\boldsymbol{S} \right|}{\int_{\partial S_i} |\boldsymbol{B}| dS} \right\rangle \rightarrow \Delta x \left\langle \frac{|\nabla \cdot \boldsymbol{B}|_i}{6|\boldsymbol{B}|_i} \right\rangle \quad \text{(Wheatland et al. 2000)}$$

  - BUT: this metric scales linearly with grid size! It is smaller for small grids
- This problem can be solved by using instead:

$$\langle |f_d| \rangle = \left\langle \frac{\left| \int_{\partial S_i} \boldsymbol{B} \cdot d\boldsymbol{S} \right|}{\int_{S_i} |\boldsymbol{B}| dV} \right\rangle = \frac{6}{\Delta x} \langle |f_i| \rangle$$

- Please take note of this – use the corrected metric!

Using chromospheric data

- The magnetic field becomes force-free in the chromosphere (Metcalf et al. 1995)
- Ideally, chromospheric vector magnetograms could be used for modeling
  - but the vector field determinations have not reached maturity
- Reliable chromospheric line-of-sight magnetograms are available: (Leka et al. 2012; Kleint 2017)
  - NSO/Synoptic Optical Long-term Investigations of the Sun (SOLIS)
  - the Interferometric BIdimensional Spectrometer (IBIS) instrument (Kleint 2017)
- ALMA measurements should also permit recovery of B_{LOS} (Loukitcheva et al. 2017)

Chromospheric constraints on NLFFF models

- Inconsistency implies the photospheric BCs must be changed to achieve an accurate solution to the NLFFF model
  - The field changes can be 100s of G (De Rosa et al. 2015)
- Chromospheric observations may be used to constrain the changes
  - Because the field there should be closer to force free
- This idea has been incorporated in the optimisation method:
  - alignment of the field at chromospheric height with fibrils (Wiegelmann et al. 2008)
  - agreement of the field, or components of the field with an observed field in a sub-volume (Fleischman et al. 2019)

Modelling the low atmosphere: insights from Bifrost

- A snapshot from a 3-D radiative MHD simulation is available (Carlsson et al. 2016)
  - a model of an enhanced network region using the Bifrost code (Gudiksen et al. 2011)
- "Photospheric" (p) and "chromospheric" (c) layers are identified (Fleishman et al. 2017)
  - plasma $\beta_p \lesssim 100$ and $\beta_c \lesssim 0.1$ at most locations at respective heights

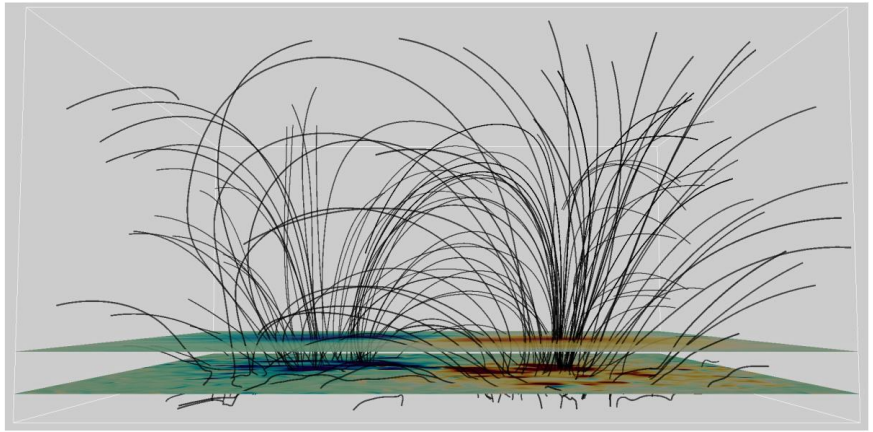

Bifrost simulation field and chosen photosphere and chromosphere (http://www.sdc.uio.no/search/simulations).

Modelling the low atmosphere: insights from Bifrost

- The simulation shows complex field variation in the p-c layer
  - some field, and most of the current, closes within the layer
    - ratio of positive flux at chromosphere to photosphere: 0.71
    - ratio of positive current at chromosphere to photosphere: 0.11

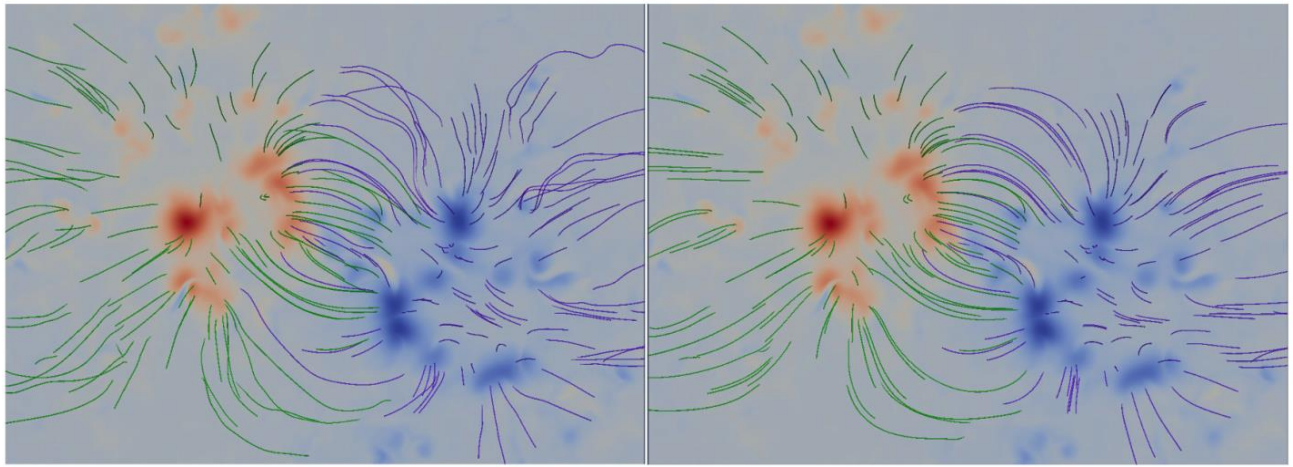

Left: Bifrost simulation field in the photosphere-chromosphere layer; right: potential field model.

Magneto-hydrostatic (MHS) extrapolation

- The low atmosphere can be modelled more accurately with the magneto-hydrostatic (MHS) model: $\boldsymbol{J} \times \boldsymbol{B} - \nabla p + \rho \boldsymbol{g} = \boldsymbol{0}$
- Optimisation, Grad-Rubin, and relaxation methods developed

  (Wiegelmann & Inhester 2003; Gilchrist & Wheatland 2013; Gilchrist et al. 2016; Miyoshi et al. 2020)

- Application to SUNRISE/IMaX data (Zhu, Wiegelmann & Solanki 2020)
  - 40km resolution – needed to model the low atmosphere from data
  - pressure BCs replaced by an estimate from $p + \frac{1}{2\mu_0} B_z^2 = \text{const}$
  - density obtained assuming constant temperature photosphere
  - Model constructed in 5Mm height box
- This suggests a two-layer modelling approach, with the chromosphere the upper boundary of the lower model (Zhu & Wiegelmann 2022)

Magneto-hydrostatic extrapolation

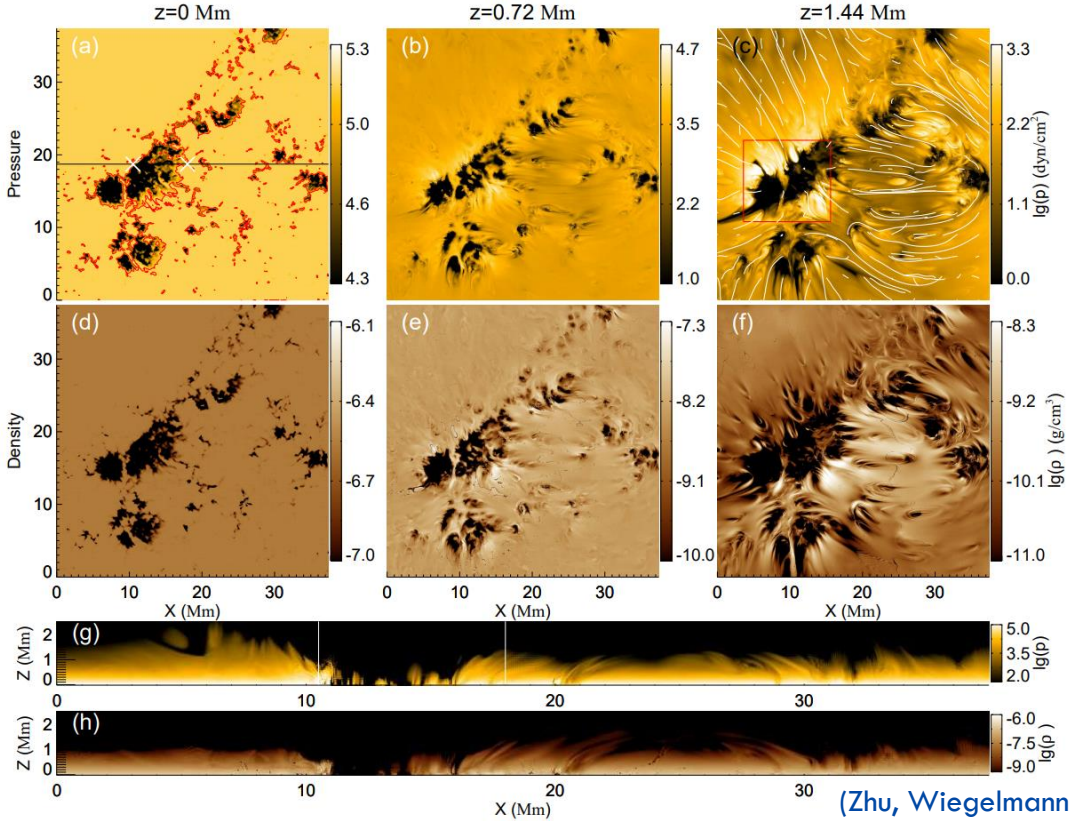

(Zhu, Wiegelmann & Solanki 2020)

Conclusions

- A hierarchy of modelling options are available
- Nonlinear force-free models have become ubiquitous
  - there is still an issue with inconsistency
- Chromospheric data may be incorporated
  - either as a constraint on NLFF models
  - or as BCs for magneto-hydrostatic modelling